Multirate Consensus-Based Distributed Control for Large-Scale Wind Farms

Jean Gonzalez Silva, Twan Keijzer, Alexander Julian Gallo, *Member, IEEE*, Riccardo Ferrari, *Senior Member, IEEE*, and Jan-Willem van Wingerden, *Senior Member, IEEE*

***Abstract*— High penetration of wind energy is pushing wind farms (WFs) to offer grid support capabilities, such as active power tracking. One of the main challenges in active power tracking for WFs is the interaction of wind turbines (WTs) through their wakes. This reduces the available wind in downstream WTs, leading them to saturation, while also affecting structural loading. With the increasing number of WTs in individual WFs, the computational and communication complexity of implementing centralized control architectures grows, posing challenges for real-world applications. In this article, we present a novel distributed control approach for active power tracking for WFs, namely multirate consensus-based distributed control (MCDC). The MCDC is designed to ensure that tracking errors caused by WT saturation are equally compensated *throughout the WF*, while only requiring local information exchanges between WTs. Furthermore, the proposed controller ensures that WT aerodynamic loading is balanced across the WF in a distributed manner. Finally, the overall power reference is distributed via a leader–follower consensus algorithm, resulting in a fully distributed approach. Our control approach facilitates the WF *modularity* and *sparsity*, which reduces the costs associated with control design and its applicability. Throughout this article, we demonstrate the effectiveness of the proposed MCDC through high-fidelity simulations, presenting performance comparable to the centralized control.**

***Index Terms*— Active power control, average consensus, distributed control, integral control, thrust balance, wake effects, wind farm (WF) control.**

I. Introduction

With the increasing share of renewable energy, concerns about power system stability become more pressing [1]. This demands further research in developing control algorithms that enable wind farm (WF) owners to effectively meet the requirements of future regulations. These regulations are evolving to support the seamless integration of WFs into power grids, moving from turbine power maximization to tracking [2], [3]. Power tracking controllers [4], [5] provide WF operators with tracking capabilities that are closer to those of conventional energy sources, enabling them to offer ancillary services to the grid [6], including frequency regulation, such as using frequency droop control schemes [7]. The integration of wind energy into the grid is stipulated by specific grid codes in each country [8], [9]. In this work, we focus on active power control, which enables the provision of these services.

Additionally, power tracking controllers can be designed to simultaneously achieve secondary WF objectives, such as balancing structural loading [10], [11], thus permitting operators to better manage the WF's resources. We have proposed a WF controller that enhances power tracking capability and distributes the aerodynamic loading [12]. However, several challenges in WF control stem from the large number of involved wind turbines (WTs). Transmitting and receiving information from hundreds of WTs in a single node at a required rate is unfavorable. In addition, the computation effort required by centralized controllers of large-scale WFs can be significantly high, as observed in [13], [14], and [15]. Therefore, facing applicability to large-scale WFs, we move from a centralized to a distributed control. Benefiting from the current turbine hardware, our proposed distributed control approach is implemented in individual WTs and resolves WF objectives by communicating only with neighbor WTs. Particularly, our approach distinguishes itself from others by consolidating all WF information at each WT before taking action.

A. WF Control and Its Reliance on Wake Modeling

As a WT extracts energy from the wind, it reduces the downstream wind velocity and adds turbulence to the flow. The altered flow is called the wake of a WT. Under the wake, downstream WTs suffer from insufficient energy availability and additional loads [16]. When WTs are not capable of producing the required amount of power, that is, the maximum power that can be produced is below the reference level set, we have the so-called turbine *saturation*.

Several design methods for WF controllers have been proposed in the literature, including those in [17] and [18], with strategies focusing on power maximization being tested in the field [19], [20]. Wake steering through yawing has been developed and utilized to maximize WF power output. However, in the context of on-demand energy, yaw misalignment could also be used to track a power demand, though it increases structural loads at the yawed turbine. Research in this area is still in its early stages [21], [22], along with emerging strategies, such as wake mixing [23]. Here, we manage the WF through the power distribution across the turbines, generally

Received 18 November 2024; revised 18 November 2024 and 10 February 2025; accepted 22 February 2025. Date of publication 2 April 2025; date of current version 20 August 2025. This work was supported by the European Union Horizon 2020 Research and Innovation Programme through Project WATEREYE under Grant 851207 and through Project TWAIN under Grant 101122194. Recommended by Associate Editor M. Abbaszadeh. *(Corresponding author: Jean Gonzalez Silva.)*

The authors are with Delft Center for Systems and Control, Delft University of Technology, 2628 CD Delft, The Netherlands (e-mail: J.GonzalezSilva@tudelft.nl; T.Keijzer@tudelft.nl; A.J.Gallo@tudelft.nl; R.Ferrari@tudelft.nl; J.W.vanWingerden@tudelft.nl).

Digital Object Identifier 10.1109/TCST.2025.3550033

referred to as *axial induction control*, keeping the turbines aligned with the wind.

To design WF controllers, engineers and researchers have modeled the WF with analytical steady-state models [24]. However, these models can demonstrate low accuracy through the validation by measurement data, as reported in [20]. The accurate modeling of wake effects is a nontrivial task to achieve because of the dynamic time-varying nature and uncertainty of the flow. The reliance on a wake model is, therefore, compromised. However, it is crucial to account for the wind flow interactions between WTs [25]. Instead of relying on WF models in an open loop, we adopt a real-time feedback WF control framework to ensure that the WF meets its objectives according to its current conditions.

B. Shift From Centralized to Distributed WF Controllers

The implementation of centralized controllers in large-scale systems poses challenges, such as communication overhead, network topology constraints, and computation effort [26]. Additionally, central approaches are susceptible to a single point of failure and often lack the flexibility to include new agents or remove failed ones without redesigning the controller, making them unsuitable for plug-and-play solutions. On the other hand, distributed control approaches, where networked local controllers are in charge of regulating parts of the entire farm, achieve *modularity* and *sparsity*. From an economic standpoint, distributed control systems are advantageous for large-scale WFs mainly attributed to the fact that each WT is not required to communicate to all other WTs, that is, all-to-all communication, or a central computational unit that might be far apart. Therefore, equipping WTs with controllers capable of achieving global WF objectives can reduce significantly the costs associated with the required communication.

The future outlook for WF control envisions a shift toward decentralization, resembling the applications seen in microgrids [27], [28] and power systems [29], [30]. Wald et al. [15] and Bay et al. [31] proposed algorithms to integrate the contribution of building energy systems and charging stations to the grid in a distributed manner. Dörfler et al. [32] proposed controllers for power systems going from a fully decentralized to a distributed control that results in an improvement in the damping of dominant oscillations. Moreover, robustness against failures in the control system can be achieved with distributed methods [33], in which local failures can be detected [34] and compensated for.

Among the first works toward distributed control in WFs are the works from Marden et al. [35] and Gebraad and van Wingerden [36]. In their works, the WT actions take into consideration their neighbor WTs. Avoiding a centralized controller, [37] and [38] maximize power production of the wind power plant using data-driven and learning approaches. Annoni et al. [39] estimated the wind speed direction using an average consensus algorithm. Finally, coalitional control, a strategy where controllers are temporarily clustered into alliances, so-called *coalitions*, jointly achieve a control objective [26], applied to WFs in [14]. Also, clusters of turbines are identified in [40], which hinges on the correlation observed in the measured power signals, for yaw control.

WF control is implemented with large sampling times because WTs should respond gradually to wind conditions. This approach helps prevent high-frequency signals from impacting the WTs, ensuring stable WT controllers. Additionally, the energy market generally does not demand immediate adjustments. However, this poses challenges for distributed WF controllers, as their convergence can be sluggish due to the distributed network topology and the extended sampling rates. As a result, responses to issues such as turbine saturation or failures may be delayed and inefficient.

C. Our Contributions

In this article, we design a distributed WF controller to achieve the following objectives.

1) O1: Regulate the WF's active power generation to track a time-varying set point.
2) O2: Distribute the WT power reference through the WF.
3) O3: Achieve aerodynamic load balancing as a surrogate for structural loading.

To reduce the communication range while maintaining a lower WF control sampling rate and still attaining performance levels akin to centralized controllers [12], the WTs are suggested to engage in high-rate communication based on a multirate scheme [41], [42]. Our approach takes advantage of the low WF sampling rate and employs average consensus [43], [44] to estimate the entire WF information before taking action. This contrasts with typical distributed methods, such as the distributed averaging proportional and integral control [30] and the distributed model predictive control [45], that consider only the information of the neighbor turbines, that is, partial information, to compute and implement local actions. Hence, we refer to our novel framework as multirate consensus-based distributed control (MCDC). The MCDC aims to achieve the objectives O1–O3, thereby counteracting power losses mainly attributed to wake effects and reaching balance in thrust forces across the WF. With the entire WF information being estimated through the communication network, this proposed method enables a distributed framework to achieve performance comparable to that of centralized approaches while using a lower WF control sampling rate.

To attain the WF objectives, the following steps are taken.

1) S1: Objective O1 is achieved by cooperatively compensating for power losses stemming from low wind availability caused by, for example, wake effects. The rationale for the power compensation is to account for this disturbance by altering the set-point of those WTs with excess available power, thus achieving WF-level reference tracking. The average of the WT power tracking errors is estimated by a high-frequency average consensus algorithm, and compensated at a lower sampling rate. By doing this, the total power tracking error is estimated at each turbine and compensated throughout the entire WF.
2) S2: To achieve O2, we implement a leader–follower consensus algorithm to distribute the global power reference across the WF, solving the alignment problem. This

power reference distribution eliminates the necessity of a central connection point for the power distribution.

3) S3: Finally, O3 is attained by computing the average aerodynamic loads through a consensus algorithm and then regulating the local aerodynamic loads to the obtained average. Treating aerodynamic loads as a surrogate of WT structural loading, the balance of aerodynamic loads leads to uniform degradation of WTs. Moreover, implementing thrust force balancing can avoid WT saturation, which may, in turn, increase the WF's total available power, compared to uniform power distribution.

The main contributions of this work include the development of the MCDC framework, a distributed approach that achieves the objectives outlined in O1–O3, the provision of stability conditions for designing the proposed MCDC scheme, and a comparison of MCDC with the centralized approach in a high-fidelity environment.

The structure of this article is as follows. First, the WF control problem will be formulated in Section II. Second, the proposed distributed control, namely MCDC, for power compensation, power distribution, and thrust balance is presented in Section III. In Section IV, simulation results will be presented using a high-fidelity simulator to evaluate the proposed controller. Lastly, conclusions and future works will be discussed in Section V.

II. Problem Formulation

In this section, before introducing the proposed MCDC, we present the simplified WF model, followed by the WF control problem. Finally, the existing centralized control design.

A. WF Model

We model the WF as a linear time-invariant dynamic system, composed of n WTs. Despite the nonlinear open-loop dynamics of WT systems, each turbine is equipped with a dedicated feedback controller designed to track a reference power setpoint. This local controller leads the WTs to exhibit predominantly linear and stable behavior. The WT controller employs both blade pitching and generator torque to regulate the power generation, as presented in [12]. Then, we take this set of controlled WT as linear systems to be regulated by the WF controller. A similar procedure has been utilized in chemical processes [46], where a linear behavior is induced in the closed-loop system, allowing for higher-level control via linear methods. Linear controllers are widely used in the industry. While the system may encounter disturbances and exhibit nonlinear behaviors, linear control methods provide robust performance and yield satisfactory results. Poor adherence of the controller WT model to reality is compensated for by the WF controller.

We applied system identification to obtain the linear dynamic model of the controlled WTs based on numerical simulation data. Step responses of generator power and thrust force to the reference power setpoint were used in the gray-box model identification process. The models are defined as single-input and multioutput (SIMO) systems, described by

$$\begin{bmatrix} P_{g,i}(k+1) \\ F_{T,i}(k+1) \end{bmatrix} = \begin{bmatrix} a_P & a_{P,T} \\ a_{T,P} & a_T \end{bmatrix} \begin{bmatrix} P_{g,i}(k) \\ F_{T,i}(k) \end{bmatrix} + \begin{bmatrix} b_P \\ b_T \end{bmatrix} P_{g,i}^{\text{ref}}(k) + \begin{bmatrix} q_{P,i}(k) \\ q_{T,i}(k) \end{bmatrix} \quad (1)$$

where k is the WF discrete-time index and $F_{T,i}$, $P_{g,i}$, and $P_{g,i}^{\text{ref}}$ are the thrust force, generator power output, and power reference of turbine i, respectively. The six parameters a_P, b_P, a_T, b_T, $a_{P,T}$, and $a_{T,P} \in \mathbb{R}^+$ are identified from simulation data. $q_{P,i}$ and $q_{T,i}$ represent the power and thrust force discrepancies, respectively, caused by model mismatch and possible turbine *saturation* of turbine i.

The first-order representation is adopted for both power and thrust force dynamics, simplifying the turbine responses. This choice is driven by our focus on the dominant transient characteristics to design the WF controller. The identification procedure utilized simulation data of the WT responses, including inflow turbulence and wake effects. Anticipating this, we propose WF controllers that incorporate an integral term to provide robustness against fluctuations in system parameters and model mismatches, as demonstrated in [47] and [48]. Although using higher-order models with only minor extensions in notation—by replacing the scalar model parameters with matrices—could improve fitting with sets of the responses, however, it may not provide a generalized representation because of the significant variability due to turbulence and wake effects.

At the WF level, there exists a time-scale separation between the dynamics of WTs with the power tracking controller, designed at sampling time ranging from 0.00125–0.1 s and a response time of 5–10 s, and the dynamics of wake interactions, of 100–300 s, depending on the turbine spacing and wind speed. In our study case, with the average wind inflow of 10 ms^{-1}, the rise time of the power tracking controller is about 8 s and the wake propagation takes between 120 and 225 s, approximately. Due to this time-scale separation between the WT dynamics and the wake flow dynamics, we make the following assumption.

Assumption 1 (Decoupled WF Model): Model (1) for WT i is decoupled from all other WTs. ◁

Note that, as a consequence of the definition of model (1) and Assumption 1, the disturbance signals $q_{P,i}$ and $q_{T,i}$ represent unmodeled behaviors. These include the effects from the turbulence in the flow, as well as the effects of the slow time-scale wake interaction, for example, induced wake turbulence and turbine *saturation* caused by the wind deficit [25], [49].

B. WF Control

As noted earlier, the WF controller must be designed to meet objectives O1–O3. In this section, we present a solution to achieve these objectives using feedback and feedforward strategies. From our previous discussion on the WT modeling, the generator power reference $P_{g,i}^{\text{ref}}$ acts as the sole input to the ith WT, and it is set as

$$P_{g,i}^{\text{ref}}(k) = \hat{P}_{g,i}^{\text{ref}}(k) + u_i(k) \quad (2)$$

where $\hat{P}_{g,i}^{\text{ref}}$ is the *feedforward term*, being the desired power reference for each WT and $u_i(k)$ is the *feedback term* defined to compensate for power tracking errors and to balance thrust forces across the WTs. Note that, so long as their sum adds to the global WF reference, there is some freedom in the definition of the feedforward terms; here we suppose $\hat{P}_{g,i}^{\text{ref}}$ are provided by the distribution of the power reference from objective O2. Conversely, the feedback term $u_i(k)$ is defined to achieve both objectives O1 and O3. Specifically

$$u_i(k) = u_{P,i}(k) + u_{T,i}(k) \tag{3}$$

where $u_{P,i}(k)$ is designed for power compensation and $u_{T,i}(k)$ for thrust balance.

Following the electromechanical constraint of typical turbines, the power reference signal (2), as the input of the WTs, is saturated as

$$P_{g,i}^{\text{ref}}(k) = \begin{cases} 0, & \text{if } P_{g,i}^{\text{ref}}(k) \le 0 \\ P_{g,i}^{\text{ref}}(k), & \text{if } 0 < P_{g,i}^{\text{ref}}(k) < P_{g,i}^{\text{rated}} \\ P_{g,i}^{\text{rated}}, & \text{else} \end{cases} \tag{4}$$

where $P_{g,i}^{\text{rated}}$ is the rated power of turbine i.

C. WF Control: The Centralized Case

As a benchmark solution to the design problem set in Section II-B, we now summarize the centralized controller proposed in [12]. There, an integral controller is used for the power compensation, such that

$$u_{P,i}(k) = u_{P,i}(k-1) + K_P \mathbf{1}_{1\times n} e_P(k) \tag{5}$$

where K_P is a scalar integrator gain, $\mathbf{1}_{1\times n} = [1\ 1, \ldots, 1]$ denotes a row vector of length n filled with ones, $e_P(k) = [e_{P,1}(k), e_{P,2}(k), \ldots, e_{P,n}(k)]^\intercal$, with the superscript $\intercal$ denoting transpose, is a vector containing the power tracking errors

$$e_{P,i}(k) = \hat{P}_{g,i}^{\text{ref}}(k) - P_{g,i}(k) \tag{6}$$

of all WTs. The wind-farm-wide power tracking error is the aggregation of all WT errors, that is, $e_P^{\text{total}}(k) = \mathbf{1}_{1\times n} e_P(k) = \sum_{i=1}^{n} (\hat{P}_{g,i}^{\text{ref}}(k) - P_{g,i}(k))$. The utilization of feedback control law (5) requires information from all WTs and ensures that the effort for power compensation is distributed throughout the entire farm. This even distribution is advantageous as it results in a minor impact from the increased wake generated by the compensating WTs, as proposed in [16], and overlooked by Assumption 1.

Similarly, an integral control is utilized for aerodynamic load balancing, in which

$$u_{T,i}(k) = u_{T,i}(k-1) + K_T e_{T,i}(k) \tag{7}$$

where K_T is a scalar integrator gain for the thrust force balance control and

$$e_{T,i}(k) = F_T^{\text{avg}}(k) - F_{T,i}(k) \tag{8}$$

is the thrust force error between the average of thrust forces across the WF F_T^{avg} and the thrust force $F_{T,i}$ acting on WT i. To compute F_T^{avg} the information of all thrust forces is required, as in the case of the power errors in the power compensation. We define the average matrix $W_{\text{avg}} = (1/n)\mathbf{1}_{n\times 1}\mathbf{1}_{1\times n}$ and rewrite (5) and (7) in vector form, such that

$$u_P(k) = u_P(k-1) + \bar{K}_P n W_{\text{avg}} e_P(k) \tag{9}$$

where $u_P(k) = [u_{P,1}(k), u_{P,2}(k), \ldots, u_{P,n}(k)]^\intercal$ and $\bar{K}_P = \text{diag}(K_P)$; and

$$u_T(k) = u_T(k-1) + \bar{K}_T \left(W_{\text{avg}} - I_n\right) F_T(k) \tag{10}$$

where $u_T(k) = [u_{T,1}(k), u_{T,2}(k), \ldots, u_{T,n}(k)]^\intercal$, $F_T(k) = [F_{T,1}(k), F_{T,2}(k), \ldots, F_{T,n}(k)]^\intercal$, $\bar{K}_T = diag(K_T)$, and I_n is the identity matrix of order n.

Instead of employing a centralized approach, we propose that the average power tracking error vector $e_P^{\text{avg}} = W_{\text{avg}} e_P$ and the average thrust force vector $F_T^{\text{avg}} = W_{\text{avg}} F_T$ are obtained from a consensus algorithm. Moreover, a consensus algorithm is also proposed to distribute the power references $\hat{P}_{g,i}^{\text{ref}}$, by aligning them to a leader turbine that has the information of the WF power demand.

III. Multirate Consensus-Based Distributed Control

We propose the so-called MCDC. To meet objectives O1–O3, the scheme consists of three control components: a power compensator, a power distributor, and a thrust balancer. The core idea is to reach a consensus estimate of the relevant WF states for each of the control components. This is accomplished by utilizing only neighborhood information, requiring a substantially less complex and resource-intensive WF communication network. Although local communication is engaged at a high frequency, its rate would remain constant and independent of the number of WTs on the farm. In a centralized controller, the number of communications at the central node increases with the number of turbines, eventually surpassing the communication per second at a node in our approach.

First, we introduce graph notation and the WF communication network in Section III-A, followed by the average consensus conducted in the WF control sampling time in Section III-B. Next, Section III-C delves into the distributed power compensation. Subsequently, Section III-D presents the power distribution as a fully distributed approach, and Section III-E covers the distributed thrust force balance. Finally, stability conditions for the entire control framework are derived and discussed in Section III-F.

A. Graph Notation and WF Communication Network

As mentioned previously, the centralized controller from Section II-C requires information on the entire WF to compute the feedback terms, consisting of (9) and (10). Moving toward distributed architectures, WTs no longer require communication from hundreds of WTs to one controller. Instead, they would only communicate with their neighbor WTs. Additionally, it would avoid problems if that one controller fails. In this section, we introduce some preliminaries on graph theory, used in our design, as well as

a critical assumption on the communication network linking WTs in the WF.

A graph $\mathcal{G}$ is defined as $\mathcal{G} = (\mathcal{V}, \mathcal{E})$, where $\mathcal{V} = v_1, \ldots, v_n$ is its vertex set, with $|\mathcal{V}| = n$ the number of agents, and $\mathcal{E} \subseteq \mathcal{V} \times \mathcal{V}$ its edge set. $\mathcal{L}$ is the Laplacian matrix, defined by $\mathcal{L} = \mathcal{D} - \mathcal{A}$, where $\mathcal{D} = \text{diag}(d_1, \ldots, d_n)$ is the in-degree matrix and $\mathcal{A}$ is the adjacency matrix. The diagonal elements $l_{i,j}$ of $\mathcal{L}$ are, therefore, equal to the in-degree of vertex v_i and the off-diagonal elements $l_{i,j}$ are -1 if there is an edge from vertex v_i and v_j, or 0 otherwise. The open neighborhood of v_i is defined by the set of neighbors $\mathcal{N}_i$ containing all the adjacent vertices to v_i excluding itself. A graph $\mathcal{G}$ is said to be undirected if $e_{ij} \in \mathcal{E}$ implies $e_{ji} \in \mathcal{E}$.

A communication network in a WF induces a graph $\mathcal{G}$ which shares the same topology, that is, for two vertices $v_i, v_j \in \mathcal{V}$, there exists an edge between them if the two can exchange information. We assume the following.

Assumption 2 (Connected Network): The communication network is such that the induced graph $\mathcal{G}$ is undirected and connected. ◁

By Assumption 2, any two distinct vertices of the graph $\mathcal{G}$ are connected through a path, meaning that there is always a directed spanning tree from a vertex to all other vertices in the graph. This assumption ensures that every agent can reach average consensus [43] and that the leader–follower consensus converges [44].

Consensus algorithms inherently provide robustness against packet loss, as demonstrated in [50]. Additionally, incorporating communication redundancies is crucial in the network design to enhance robustness and guarantee connectivity in the event of a communication failure from a WT. This is achieved by ensuring that each WT exchanges information with at least two others, meaning each vertex v_i has at least two connecting edges. In this case, when a link fails, consensus would still be achieved, yet the stability of the closed-loop system should be verified as it also depends on the network topology. Furthermore, switching network schemes [44] can be implemented to address these failures and optimize operations through reconfiguration. However, we assume that the turbines have no issue in sharing information.

B. Average Consensus Within the WF Control Sampling Time

Our proposed multirate controller assumes that the data exchange between WTs can occur at a higher rate than the WF control. The WF control typically operates at a low time scale, between 20 s and 10 min [6], being suitable for conducting consensus algorithms [43], [44] to estimate the relevant WF information before the WF control action's execution. This inherently leads to a unitary delay in the action, which will be further discussed and assessed. This design consideration is in line with the control of power systems, where different time scales are accounted for [30]. In this section, we present a general formulation of the consensus algorithm, used to obtain the estimates for the power compensator and thrust balancer.

The average consensus of a state $x \in \mathbb{R}^n$ is to be achieved at each WT in $h \in \mathbb{N}$ iterations, the consensus horizon. For clarity, the average consensus algorithm is divided into three stages: *(re-)initialization*; *inner iteration*; and *final assignment*.

In the *(re-)initialization*, the state variable of the average consensus, x_i^{avg} is initialized as

$$x_i^{\text{avg}}(0) = x_i(k). \tag{11}$$

Then, the *inner iteration* is recursively conducted over the consensus horizon, as follows:

$$x_i^{\text{avg}}(c+1) = w_{i,i} x_i^{\text{avg}}(c) + \sum_{j \in \mathcal{N}_i} w_{i,j} x_j^{\text{avg}}(c) \tag{12}$$

for $c \in \{0, 1, \ldots, h-1\}$, where $w_{i,i}$ is the weight on x_i^{avg} at vertex i and $w_{i,j}$ are the weights on x_j^{avg} at vertex i. As the last stage, the *final assignment* is

$$x_i^{\text{avg, final}}(k|k+1) = x_i^{\text{avg}}(h), \tag{13}$$

where $x_i^{\text{avg, final}}$ is the final average value obtained after h steps and utilized for defining the WF control action. The notation $(k|k+1)$ is utilized to highlight that the estimate of the average of $x(k)$ can only be obtained at $k+1$. By setting $w_{i,j} = 0$ for $j \notin \mathcal{N}_i$, we can then rewrite (11)–(13) in a vector form

$$x^{\text{avg}}(0) = x(k) \tag{14a}$$

$$x^{\text{avg}}(c+1) = W x^{\text{avg}}(c) \quad \forall c \in \{0, 1, \ldots, h-1\} \tag{14b}$$

$$x^{\text{avg, final}}(k|k+1) = x^{\text{avg}}(h) \tag{14c}$$

where $W = [w_{i,j}]$ is the average consensus weight matrix. The matrix W is structured to respect the communication topology and has to satisfy the following conditions:

$$\lambda_1(W) = 1 \text{ and } |\lambda_i(W)| \leq 1 \text{ for all } i = 2, \ldots, n \tag{15a}$$

$$W \mathbf{1}_{n\times 1} = \mathbf{1}_{n\times 1} \tag{15b}$$

$$\mathbf{1}_{1\times n} W = \mathbf{1}_{1\times n}. \tag{15c}$$

While average consensus is only reached in the limit, as $h \to \infty$, a suitable average can be achieved in finite iterations, by choosing a sufficiently large h. Moreover, the optimal design of W to achieve the fastest convergence rate and enhance accuracy is obtained by solving the following optimization problem, the so-called fastest discrete-time consensus (FDTC) problem [51]:

$$\text{minimize}_{w_{ij}} \rho\left(W - W_{\text{avg}}\right) \tag{16a}$$

$$\text{subject to } W\mathbf{1}_{n\times 1} = \mathbf{1}_{n\times 1}, \tag{16b}$$

$$W = W^{\intercal}, \tag{16c}$$

$$w_{i,j} = 0, \text{ if } (i,j) \notin \mathcal{E} \text{ and } i \neq j, \tag{16d}$$

where $\rho(S)$ is the spectral radius of S, and the convergence speed decreases with $\rho(S)$; and, reiterating, $W_{\text{avg}} = (1/n)\mathbf{1}_{n\times 1}\mathbf{1}_{1\times n}$ is the average matrix. Since we impose W to be symmetric as a design choice, the spectral radius of a symmetric matrix is also its spectral norm, then (16a) can be cast as the minimization of $\|W - W_{\text{avg}}\|$, where the operator $\|\cdot\|$ is the induced matrix 2-norm. This problem is convex and can be solved globally and efficiently.

Notice that for plug-and-play capabilities, the optimization problem should be reconsidered taking into account the new addition or removal to keep overall optimality. Otherwise, at least, the elements of W associated with their neighbors should be changed accordingly to maintain the conditions in (15).

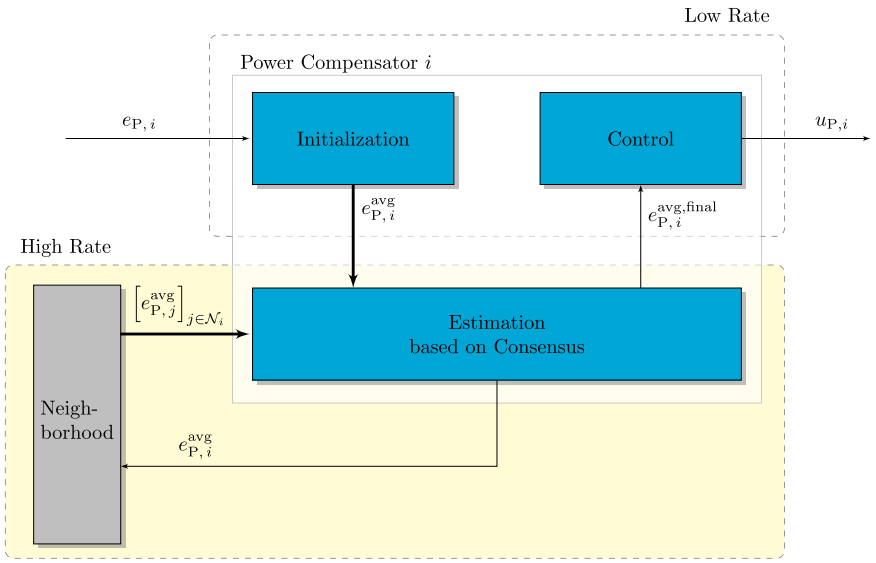

Fig. 1. Block diagram of the power compensator based on the consensus of the power errors.

C. Power Compensation

Let us now address the solution to objective O1 in a distributed manner. The main idea is to utilize WTs with enough wind resources to cooperatively compensate for power-tracking errors. This ensures that overall power tracking at the WF level can still be attained in the case of turbine *saturation*. Fig. 1 illustrates our proposed distributed strategy for power compensation. Each WT i initiates its consensus protocol based on its own power error. Then, the average power error across the entire farm is estimated through the average consensus process that communicates the power errors in a neighborhood at a high rate. Subsequently, the control computes the feedback control signal $u_{P,i}$ at a low rate using the estimates of the WF power error. This strategy is detailed as follows, divided into Estimation and Control.

1) Estimation: The first step in our distributed power compensation strategy is to estimate the WF power error. This is accomplished by computing the average power error at each WT using the average consensus algorithm, as presented in Section III-B. The algorithm leverages the current power error information at each WT and disseminates it by engaging in high-frequency communication with neighboring WTs. If Assumption 2 holds, and provided that h is sufficiently large, the average consensus value is obtained in the subsequent low-rate time step. Theoretically [43], [51], we have

$$\lim_{h\to\infty} W^h e_P(k) = W_{\mathrm{avg}} e_P(k) = e_P^{\mathrm{avg,\ final}}(k|k+1) \tag{17}$$

where e_P is the vector containing all power tracking errors of each WT, W is the average consensus weight matrix, which is structured to respect the communication topology, and W_{avg} is the average matrix. The notation $(k|k+1)$ signifies that the average of power losses $e_P^{\mathrm{avg,\ final}}$ from k is only obtained at $k+1$. This notation emphasizes the delay attained by utilizing our proposed approach. Thus, the WF power error is estimated to be $ne_P^{\mathrm{avg,\ final}}(k|k+1)$.

During the design stage, a finite value for h is determined, constrained by the speed of the communication system in transmitting information and the time required by the local controller to execute the algorithm. Since communication speed and computation time are "hard" constraints, the designer must account for some tolerance in the attained average consensus. The choice of h affects the distribution of the power compensation, moving from uniform, widespread compensation across the farm with h sufficiently large, to a more localized compensation with a low value of h. This localized compensation is acknowledged without significant prejudice, as (15b) guarantees that the sum of the vector of node values is preserved and h is factored into the stability conditions derived further in this work.

2) Control: We propose a compensation strategy following the integral method derived for centralized controller in [12] and presented in Section II-C. The integral method is demonstrated to achieve stability even with the presence of the additional step-time delay for the execution of the consensus algorithm. The control law at each WT uses the final estimated average power error $e_P^{\mathrm{avg,\ final}}(k-1|k)$ from the previous time step $k-1$ obtained at k, and it is defined as

$$u_{P,i}(k) = u_{P,i}(k-1) + K_P n e_{P,i}^{\mathrm{avg,\ final}}(k-1|k) \tag{18}$$

where K_P is the integrator gain for the power compensator. In vector form, we can rewrite (18) as

$$u_P(k) = u_P(k-1) + \bar{K}_P W_P e_P(k-1) \tag{19}$$

where $\bar{K}_P$ is the gain matrix defined as $\bar{K}_P := \mathrm{diag}(K_P)$, and $W_P = nW^h$ a weight matrix. Notice that differing from a central control law (9), the average depends on the value of h and if $h \to \infty$ then $W_P = nW_{\mathrm{avg}}$. Importantly, the computation of the average consensus adds a sampling time delay to the power error signal in (19), compared to the centralized controller in (9).

Remark 1: With the control law (18) utilizing the average consensus with a sufficiently large h, the compensation equally

spreads the additional power demand, as in the centralized approach. This equal compensation across all turbines is simple and effective. Furthermore, the compensation can be expanded to take the intensity of the turbine interactions into account in (18), for example, using a WF model-based optimization [18], or estimations of available power [13]. A weighted approach across turbines considering the intensity of the interactions is a direct extension. Our proposed controller combines power compensation with aerodynamic load balancing, accounting for interactions and promoting a power distribution that leads to uniform degradation and prevents turbine saturation. ◁

D. Power Distribution

In a fully distributed WF system, the desired power references $\hat{P}^{\text{ref}}_{g,i}(k)$, as a solution of objective O2, should also be obtained in a distributed manner. The information regarding the desired power reference for each turbine can be disseminated throughout the communication network by solving the *alignment problem* [44], also known as leader–follower consensus.

The alignment problem is accomplished by converging all the desired power references to leader turbines. The leader turbines leave their values unchanged, while all others asymptotically agree with them according to the consensus protocol, achieving alignment. The leader–follower consensus is conducted between the WF control sampling time, so it also follows the notations from Section III-B.

A widely employed benchmark approach is to divide the WF power reference uniformly among all WTs [13]. As a *feedforward term*, the desired power reference provides an initial reference to the WTs, with the primary goal of sharing implicit information on the total farm power demand, while the *feedback terms* are also incorporated into the power reference signals. For simplicity, we assume a single leader identified as the WT $i = m$. The leader's power reference is determined by dividing the total WF power reference P^{ref}_{WF} by the number of WTs in the WF such that the *(re)initialization* of the leader turbines is defined as follows:

$$P^{\text{ref, align}}_{g,m}(0) = P^{\text{ref}}_{WF}(k)/n \tag{20}$$

while the *(re)initialization* of the other turbines is

$$P^{\text{ref, align}}_{g,i}(0) = \hat{P}^{\text{ref}}_{g,i}(k-1) \quad \forall i \neq m \tag{21}$$

for $k \geq 1$, where $P^{\text{ref, align}}_{g,i}$ is the internal state variable.

Then, in the *inner iteration* stage, the leader's power reference remains constant, being

$$P^{\text{ref, align}}_{g,m}(c+1) = P^{\text{ref, align}}_{g,m}(c) \quad \forall c = 0, 1, \ldots, h-1 \tag{22}$$

where c is an internal discrete-time index. On the other hand, the followers $i \neq m$ converge to the leader as

$$\hat{P}^{\text{ref, align}}_{g,i}(c+1) = a_{i,i}\hat{P}^{\text{ref, align}}_{g,i}(c) + \sum_{j \in \mathcal{N}_i \setminus m} a_{i,j}\hat{P}^{\text{ref, align}}_{g,j}(c) + b_i P^{\text{ref, align}}_{g,m}(c) \tag{23}$$

$\forall c = 0, 1, \ldots, h-1$, where $a_{i,j} \in \mathbb{R}$ and b_i is either $\beta_i \in \mathbb{R}$ if agent i is connected to the leader, or 0 otherwise.

At the *final assignment* stage

$$\hat{P}^{\text{ref}}_{g,i}(k|k+1) = P^{\text{ref, align}}_{g,i}(h) \quad \forall i. \tag{24}$$

For a single leader, without loss of generality, we can assume that this agent is the one labeled with $m = n$. Then, the multiagent system is said to achieve alignment between the WF control sampling time when

$$\lim_{h \to \infty} ||\hat{P}^{\text{ref}}_{g,i}(k|k+1) - \hat{P}^{\text{ref}}_{g,n}(k|k+1)|| = 0 \tag{25}$$

$\forall i \in \{1, 2, \ldots, n-1\}$. The *inner iteration* defined by (22) and (23) can be written in state form as

$$\begin{bmatrix} P^{\text{ref, align}}_{i=1:n-1}(c+1) \\ P^{\text{ref, align}}_{n}(c+1) \end{bmatrix} = \underbrace{\left[\begin{array}{c|c} A_{\text{lf}} & B_{\text{lf}} \\ \hline 0_{1\times n-1} & 1_{1\times 1} \end{array}\right]}_{L_{\text{lf}}} \begin{bmatrix} P^{\text{ref, align}}_{i=1:n-1}(c) \\ P^{\text{ref, align}}_{n}(c) \end{bmatrix} \tag{26}$$

$\forall c = 0, 1, \ldots, h-1$, where $A_{\text{lf}} = [a_{i,j}]_{n-1\times n-1}$, with $a_{i,j} = 0$ for $j \notin \mathcal{N}_i$, and $B_{\text{lf}} = [b_1, b_2, \ldots, b_{n-1}]^\intercal$. The design of the parameters $a_{i,j}$ and $b_i \in \mathbb{R}$ is conducted by an equivalency with the alignment problem derived in [44]. It then follows:

$$A_{\text{lf}} = \left(I_{n-1} + \mathcal{D}_{n-1\times n-1} + B'\right)^{-1}\left(I_{n-1} + \mathcal{A}_{n-1\times n-1}\right) \tag{27}$$

$$B_{\text{lf}} = \left(I_{n-1} + \mathcal{D}_{n-1\times n-1} + B'\right)^{-1} B' \tag{28}$$

where B' is an $n-1 \times n-1$ diagonal matrix whose ith diagonal element is 1, if i is the neighbor of the leader, and 0 otherwise; $\mathcal{D}_{n-1\times n-1}$ and $\mathcal{A}_{n-1\times n-1}$ are the degree and adjacency matrices removing the last column and row, respectively. In this way, L_{lf} in (26) is an stochastic matrix, that is, $L_{\text{lf}}\mathbf{1}_{n\times 1} = \mathbf{1}_{n\times 1}$ and L_{lf} is square with all entries nonnegative.

Utilizing this approach, the distribution of WF power reference is not made by a central workstation to each turbine, as typically observed in the general centralized scenario. Instead, the communication is distributed in exchange for a time-step delay. This time-step delay, on the other hand, can be designed to be as small as necessary, constrained by the execution of the consensus algorithm.

E. Thrust Balance Control

Following objective O3, we aim to evenly distribute the thrust forces throughout the entire farm in a distributed manner. Our solution in this section also takes advantage of the average consensus and the time-scale separation from the WF and WT controllers to compute the average thrust forces.

For computing the feedback control signal $u_{T,i}(k)$, we use the average thrust force across the entire farm obtained from average consensus estimates.

1) Estimation: The thrust force errors are estimated by computing the average thrust force across the WF at each WT employing the average consensus algorithm from Section III-B. The thrust force tracking errors $e_{T,i}$ is defined as

$$e_{T,i}(k) = F^{\text{avg}}_{T,i}(k) - F_{T,i}(k) \tag{29}$$

where $F^{\text{avg}}_{T,i}$ is the average of thrust force known at the ith WT and $F_{T,i}$ is the current thrust force. Different from the

centralized controller, $F_{T,i}^{\text{avg}}$ is computed across the WF by the average consensus algorithm from Section III-B, such that the estimations of the thrust force errors are defined as

$$e_T(k-1|k) = \left(W^h - I_n\right)F_T(k-1) = -W_T F_T(k-1) \quad (30)$$

where $W_T = -(W^h - I_n)$. When $h \to \infty$

$$e_T(k-1|k) = \left(W_{\text{avg}} - I_n\right)F_T(k-1). \quad (31)$$

This indicates that the strategy introduces a sampling time delay besides the consensus algorithm being conducted with a finite h in practice. Similar to the power compensation, the choice of h dictates the level of smoothness in the averaging of the thrust forces across the WF.

2) Control: The control protocol that balances the thrust force is proposed to be composed of pure integrators. The sampling time delay originating from the computation of the average consensus is embedded into the proposed control law (32) by considering the definition of the error signals from (30), contrasting with the central control law in (7)

$$u_{T,i}(k) = u_{T,i}(k-1) + K_T e_{T,i}(k-1|k) \quad (32)$$

which can be rewritten in a vector form as

$$\begin{aligned} u_T(k) &= u_T(k-1) + \bar{K}_T e_T(k-1|k) \\ &= u_T(k-1) - \bar{K}_T W_T F_T(k-1) \end{aligned} \quad (33)$$

where $\bar{K}_T = \text{diag}(K_T)$.

Remark 2: Note that the weight matrix W_T is a double-stochastic matrix by definition, and, therefore, it guarantees that $\sum_i u_{T,i}(k) = 0\,\forall k$. Indeed, from (33)

$$\sum_i u_{T,i}(k) = \mathbf{1}_{1\times n} u_T(0) \; - \sum_{\tau=1}^{k} \mathbf{1}_{1\times n}\bar{K}_T W_T F_T(\tau-1). \quad (34)$$

Thus, provided that $u_{T,i}(0) = 0\ \forall i$ is established as the initial condition for the integrators, $\mathbf{1}_{1\times n}\bar{K}_T W_T F_T(k-1) = 0\ \forall k$ is a sufficient condition for $\sum_i u_{T,i}(k) = 0\,\forall k$. Thus, by the definition of W_T

$$\mathbf{1}_{1\times n}\bar{K}_T W_T F_T(k-1) = 0 \quad (35)$$

holds, where $\mathbf{1}_{1\times n} W_T = 0_n$ follows from the definition of $W_T = -(W^h - I_n)$, as W^h is a double-stochastic matrix. ◁

Remark 3: When turbine saturation[1] occurs in one of the WTs, the balancing of thrust forces would reduce the total WF power generation. The saturated turbine cannot increase power generation and it typically has a lower thrust force compared to the remaining turbines. Consequently, the saturated turbine affects the power generation of the other turbines by diminishing their power output and failing to compensate for their reduced generation with its own increased power generation. Hence, we exclude saturated turbines from the balancing of thrust forces, departing from the previous practice in the central approach in [11] and [12]. This prioritizes object O1 and is justified by the fact that the thrust forces of saturated turbines are lower than the remaining ones. To accomplish this, we define the consensus algorithm, such that W^h reaches the definition of the average matrix in (36) when $h \to \infty$

$$W_{\text{avg, sat}} = \left[w_{i,j}\right] = \begin{cases} 1, & \text{if } i = j \text{ is saturated} \\ 0, & \text{if } i \neq j \text{ and } i \text{ or } j \text{ is saturated} \\ \dfrac{1}{n - n_S}, & \text{otherwise} \end{cases} \quad (36)$$

where n_S is the number of saturated turbines. The saturation information is also obtained through average consensus, thereby maintaining distributed communication. Since this follows directly from Section III-B, it is omitted for brevity. The double-stochasticity property in (36) persists and the result thrust force error of the saturated turbines is zero, granting an anti-windup property for the integrators. ◁

Remark 4: In the event of a scheduled shutdown for maintenance at specific WTs, the power compensation and power distribution, as discussed in Sections III-C and III-D, could remain unchanged. In this way, the power error at the shutdown turbine will be compensated by the other from the feedback loop. The information about the turbine to be shut down can be transmitted through the communication network by the alignment consensus algorithm. The turbine undergoing shutdown must be removed from the thrust force balancing and this can be handled in the same manner as when turbine saturation occurs, following (36). ◁

F. Stability of the Proposed MCDC Scheme

To start the discussions in this section, we consider the concept of bounded input bounded output (BIBO) stability and how it relates to turbine saturation in the farm. Here, exogenous inputs, that is, the references $\hat{P}_g^{\text{ref}}$, and the disturbances q_P and q_T, are acknowledged as bounded, as substantiated by the following assessments.

1) The contribution of the inflow turbulence or other unmodelled effects is bounded, such that $|q_{P,i}| < K_1$ and $|q_{T,i}| < K_2$ for all i, where K_1 and $K_2 \in \mathbb{R}$, governed by the convergence of the dedicated feedback controller at each WT.
2) Owing to potential saturation $q_{P,i} < 0$ and $q_{P,i} \geq -P_{g,i}^{\text{rated}}$, as a result of the constraints imposed by the turbines and the reference signal, $P_{g,i} \geq 0$, $P_{g,i}^{\text{ref}} \geq 0$, and $P_{g,i}^{\text{ref}} \leq P_{g,i}^{\text{rated}}$; and, similarly, $q_{T,i} < 0$, and $q_{T,i} \geq -F_{T,i}^{\max}$, where $F_{T,i}^{\max}$ is the maximum thrust force admitted by an individual WT.

For the closed-loop system to be BIBO stable, meaning that the norms of the power and thrust force errors remain bounded for bounded inputs, a necessary condition is that the poles of the closed-loop system must be in a stable region. From (1), the dynamics of the power generation and thrust force are rewritten in vector form as

$$P_g(k+1) = A_P P_g(k) + A_{T,P} F_T(k) + B_P P_g^{\text{ref}}(k) + q_P(k) \quad (37)$$

[1]Turbine saturation refers to a condition where a turbine operates at maximum capacity and cannot produce any more power when demanded. This condition is imposed by unavailable wind and/or high demand.

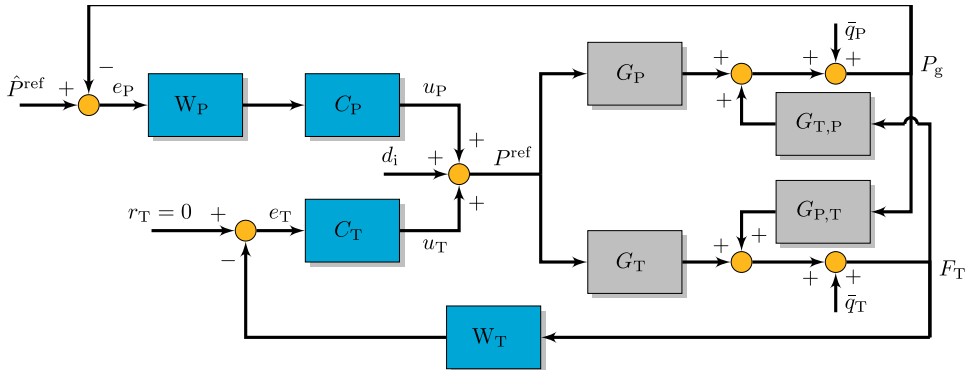

Fig. 2. Block diagram of the closed-loop system with both feedback loops. The communication is represented by W_P and W_T.

$$F_T(k+1) = A_T F_T(k) + A_{P,T} P_g(k) + B_T P_g^{\text{ref}}(k) + q_T(k) \tag{38}$$

where, given Assumption 1, $A_P = \text{diag}(a_P)$, $A_{T,P} = \text{diag}(a_{T,P})$, and $B_P = \text{diag}(b_P)$; and $A_T = \text{diag}(a_T)$, $A_{P,T} = \text{diag}(a_{P,T})$, and $B_T = \text{diag}(b_T)$. Thus, we convert (37) and (38) from their discrete-time description to the z-domain [52] and reorganize them using matrix algebra

$$\begin{aligned} P_g &= (I_n z - A_P)^{-1}\left(A_{T,P} F_T + B_P P_g^{\text{ref}} + q_P\right) \qquad (39)\\ &= G_{T,P} F_T + G_P P_g^{\text{ref}} + G_{P,q} q_P \\ F_T &= (I_n z - A_T)^{-1}\left(A_{P,T} P_g + B_T P_g^{\text{ref}} + q_T\right) \qquad (40)\\ &= G_{P,T} P_g + G_T P_g^{\text{ref}} + G_{T,q} q_T \end{aligned}$$

where P_g, F_T, $\hat{P}_g^{\text{ref}}$, q_P, and q_T represent the Z-transform of the respective vectors from this point, calculated as $Z[x(k+a)] = z^a x(z)$ with $a \in \mathbb{Z}$; and $G_{T,P} = (I_n z - A_P)^{-1} A_{T,P}$, $G_P = (I_n z - A_P)^{-1} B_P$, $G_{P,q} = (I_n z - A_P)^{-1}$, $G_{P,T} = (I_n z - A_T)^{-1} A_{P,T}$, $G_T = (I_n z - A_T)^{-1} B_T$, $G_{T,q} = (I_n z - A_T)^{-1}$ are defined transfer functions. For simplicity, we denote $\bar{q}_P = G_{P,q} q_P$ and $\bar{q}_T = G_{T,q} q_T$. Replacing (39) and (40) into each other and rearranging the terms, we have the following representation of the WF dynamics:

$$\begin{aligned} P_g &= \left(I_n - G_{T,P} G_{P,T}\right)^{-1} \\ &\quad \times \left[\left(G_P + G_{T,P} G_T\right) P_g^{\text{ref}} + G_{T,P} \bar{q}_T + \bar{q}_P\right] \qquad (41)\\ F_T &= \left(I_n - G_{P,T} G_{T,P}\right)^{-1} \\ &\quad \times \left[\left(G_T + G_{P,T} G_P\right) P_g^{\text{ref}} + G_{P,T} \bar{q}_P + \bar{q}_T\right]. \qquad (42) \end{aligned}$$

Furthermore, we also convert the power reference input signal to the Z-domain, which incorporates the control laws previously defined in (19) and (33), such that

$$\begin{aligned} P_g^{\text{ref}} &= \hat{P}_g^{\text{ref}} + u_P + u_T \qquad (43)\\ u_P &= (I_n z - I_n)^{-1} \bar{K}_P W_P e_P = C_P W_P\left(\hat{P}_g - P_g\right) \qquad (44)\\ u_T &= (I_n z - I_n)^{-1} \bar{K}_T e_T = C_T W_T F_T \qquad (45) \end{aligned}$$

where u_P, u_T, e_P, and e_T represent the Z-transform of the respective vectors from this point forward, and $C_P = (I_n z - I_n)^{-1} \bar{K}_P$, $C_T = (I_n z - I_n)^{-1} \bar{K}_T$ are the defined control transfer functions. To emphasize, these control transfer functions represent a backward numerical integration due to the delay inherent in our approach, contrasting with the forward integration used in centralized control.

The feedback system is illustrated in the block diagram in Fig. 2. In this representation, the input disturbance d_i includes the feedforward term, which is the reference power $\hat{P}_g^{\text{ref}}$, an exogenous signal. To assess stability, we close both feedback loops using the system equations (41) and (42), along with the control signal (43). Consequently, we can formulate the following theorem.

Theorem 1: The closed-loop stability, utilizing both feedback control laws (44) and (45) simultaneously, is ensured when the following matrix inequalities are satisfied:

$$A_0 - A_3 < 0, \tag{46a}$$

$$A_0 + A_1 + A_2 + A_3 > 0 \tag{46b}$$

$$A_0 - A_1 + A_2 - A_3 < 0 \tag{46c}$$

and

$$A_3^2 - A_0^2 + A_0 A_2 - A_1 A_3 > 0 \tag{47}$$

where $A_3 = I_n$, $A_2 = -(I_n + A_P + A_T)$, $A_1 = A_P A_T + A_P + A_T + A_{T,P} A_{P,T} + B_P \bar{K}_P W_P + W_T B_T \bar{K}_T$, $A_0 = -A_P A_T + A_{T,P} A_{P,T} - A_T B_P \bar{K}_P W_P + A_{T,P} B_T \bar{K}_P W_P - A_P W_T B_T \bar{K}_T + A_{P,T} W_T B_P \bar{K}_T$, and $|.|$ is the determinant operation.

Proof: Taking (43), and replacing with the control laws (44) and (45), and subsequently replacing with (41) and (42), we have

$$\begin{aligned} P_g^{\text{ref}} &= \hat{P}_g^{\text{ref}} + u_P + u_T \qquad (48a)\\ &= \hat{P}_g^{\text{ref}} + C_P W_P\left(\hat{P}_g^{\text{ref}} - P_g\right) - C_T W_T F_T \qquad (48b)\\ &= \left(I_n + C_P W_P\right) \hat{P}_g^{\text{ref}} - C_P W_P \left(I_n - G_{T,P} G_{P,T}\right)^{-1} [(G_P \\ &\quad + G_{T,P} G_T) P_g^{\text{ref}} + G_{T,P} \bar{q}_T + \bar{q}_P] \\ &\quad - C_T W_T \left(I_n - G_{P,T} G_{T,P}\right)^{-1} \\ &\quad \left[\left(G_T + G_{P,T} G_P\right) P_g^{\text{ref}} + G_{P,T} \bar{q}_P + \bar{q}_T\right] \qquad (48c)\\ &= \Big[I_n + C_P W_P \left(I_n - G_{T,P} G_{P,T}\right)^{-1} \left(G_P + G_{T,P} G_T\right) \\ &\quad + C_T W_T \left(I_n - G_{P,T} G_{T,P}\right)^{-1} \left(G_T + G_{P,T} G_P\right)\Big]^{-1} \\ &\quad \left\{\left(I_n + C_P W_P\right) \hat{P}_g^{\text{ref}} - C_P W_P \tilde{q}_P - C_T W_T \tilde{q}_T\right\}. \qquad (48d) \end{aligned}$$

From (48c) to (48d), we rearranged (48c) by isolating the power reference P_g^{ref} and we denote $\tilde{q}_P = (I_n - G_{T,P} G_{P,T})^{-1}$

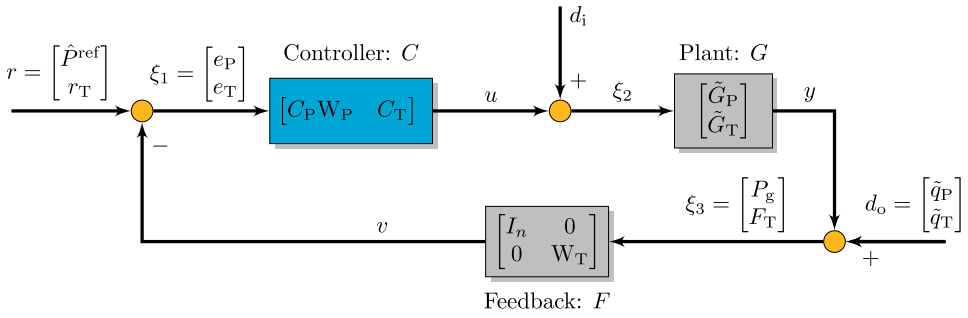

Fig. 3. Block diagram of the closed-loop system in a basic feedback loop representation.

$(G_{T,P}\bar{q}_T + \bar{q}_P)$ and $\tilde{q}_T = (I_n - G_{P,T}G_{T,P})^{-1}(G_{P,T}\bar{q}_P + \bar{q}_T)$, having stable relationships with $\bar{q}_P$ and $\bar{q}_T$ by the definitions of $G_{P,T}$ and $G_{T,P}$. Substituting the transfer functions accordingly and utilizing algebraic manipulations, the inverse term that includes the closed-loop characteristic equation becomes

$$\begin{aligned}&\Big[I_n + C_P W_P\big(I_n - G_{T,P}G_{P,T}\big)^{-1}\big(G_P + G_{T,P}G_T\big) + C_T W_T (I_n \\ &\quad - G_{P,T}G_{T,P}\big)^{-1}\big(G_T + G_{P,T}G_P\big)\Big]^{-1} \\ &= [(I_n z - A_P)(I_n z - A_T) \\ &\quad (I_n z - I_n) - (I_n z - I_n)A_{T,P}A_{P,T} + (I_n z - A_T)\bar{K}_P W_P B_P \\ &\quad + A_{T,P}\bar{K}_P W_P B_T + (I_n z - A_P)\bar{K}_T W_T B_T + A_{P,T}\bar{K}_T W_T B_P\Big]^{-1} \\ &\quad \big[(I_n z - A_P)(I_n z - A_T) - A_{T,P}A_{P,T}\big](I_n z - I_n).\end{aligned}$$

To ensure stability, we must guarantee that the solutions to the characteristic matrix polynomial

$$\begin{aligned}&\det\big((I_n z - A_P)(I_n z - A_T)(I_n z - I_n) - (I_n z - I_n)A_{T,P}A_{P,T} \\ &\quad + (I_n z - A_T)\bar{K}_P W_P B_P + A_{T,P}\bar{K}_P W_P B_T \\ &\quad + (I_n z - A_P)\bar{K}_T W_T B_T + A_{P,T}\bar{K}_T W_T B_P\big) = 0. \qquad (49)\end{aligned}$$

lie within the unit circle. To demonstrate this, we rely on the multivariate extension of the Jury stability criterion [53], as presented in [54]. Specifically, let us start by defining $Q(z) = (I_n z - A_P)(I_n z - A_T)(I_n z - I_n) - (I_n z - I_n)A_{T,P}A_{P,T} + (I_n z - A_T)\bar{K}_P W_P B_P + A_{T,P}\bar{K}_P W_P B_T + (I_n z - A_P)\bar{K}_T W_T B_T + A_{P,T}\bar{K}_T W_T B_P$. Then, $\det(Q(z)) = 0$ has a solution only if $\exists x \neq 0$ such that $x^\top Q(z)x = 0$.[2] Thus, solving (49) and verifying its solutions is equivalent to evaluating

$$\begin{aligned}&x^\top Q(z)x \\ &= x^\top[(I_n z - A_P)(I_n z - A_T)(I_n z - I_n) \\ &\quad - (I_n z - I_n)A_{T,P}A_{P,T} + (I_n z - A_T)\bar{K}_P W_P B_P \\ &\quad + A_{T,P}\bar{K}_P W_P B_T + (I_n z - A_P)\bar{K}_T W_T B_T + A_{P,T}\bar{K}_T W_T B_P\big]x \\ &= x^\top\big[I_n z^3 - (I_n + A_P + A_T)z^2 + (A_P A_T + A_P + A_T \\ &\quad + A_{T,P}A_{P,T}\bar{K}_P W_P B_P + \bar{K}_T W_T B_T\big)z - A_P A_T + A_{T,P}A_{P,T} \\ &\quad - A_T\bar{K}_P W_P B_P + A_{T,P}B_T\bar{K}_P W_P \\ &\quad - A_P\bar{K}_T W_T B_T + A_{P,T}W_T B_P\bar{K}_T\big]x \\ &= x^\top A_3 x z^3 + x^\top A_2 x z^2 + x^\top A_1 x z + x^\top A_0 x = 0 \qquad (50)\end{aligned}$$

[2]For any matrix $A \in \mathbb{R}^{n\times n}$, $\det(A) = 0$ is equivalent to $\text{rank}(A) < n$ and, therefore, $\text{nullity}(A) = \dim(\ker(A)) \geq 1$. This latter fact implies that $\exists x \neq 0 \in \mathbb{R}^n$ s. t. $x \in \ker(A) \implies Ax = 0 \implies v^\top Ax = 0, \forall v \in \mathbb{R}^n$. Taking $v = x$, $x^\top Ax = 0$.

where $A_3 = I_n$, $A_2 = -(I_n + A_P + A_T)$, $A_1 = A_P A_T + A_P + A_T + A_{T,P}A_{P,T} + B_P\bar{K}_P W_P + W_T B_T\bar{K}_T$, $A_0 = -A_P A_T + A_{T,P}A_{P,T} - A_T B_P\bar{K}_P W_P + A_{T,P}B_T\bar{K}_P W_P - A_P W_T B_T\bar{K}_T + A_{P,T}W_T B_P\bar{K}_T$. Then, it is possible to exploit the Jury stability criterion [53]. Having solutions of $\det(Q(z)) = 0$ restricted to the complex unit disk is equivalent to satisfying the stability constraints of the third-order polynomial (50), such that

$$\begin{cases} x^\intercal(A_3 + A_2 + A_1 + A_0)x > 0, & (51a) \\ x^\intercal(A_3 - A_2 + A_1 - A_0)x > 0, & (51b) \\ x^\intercal(A_3 - A_0)x > 0, \text{ and} & (51c) \end{cases}$$

$$\begin{vmatrix} x^\intercal A_0 x & x^\intercal A_1 x \\ x^\intercal A_3 x & x^\intercal A_2 x \end{vmatrix} - \begin{vmatrix} x^\intercal A_0 x & x^\intercal A_3 x \\ x^\intercal A_3 x & x^\intercal A_0 x \end{vmatrix} > 0. \qquad (52)$$

In turn, given that A_3, A_2, A_1, A_0 are symmetric by construction, the conditions in (51a) are equivalent to the linear matrix inequalities in (46); and (52) equivalent to (47). ■

The stability conditions from Theorem 1 imply internal stability for our proposed MCDC framework in our study case, which we evaluate through the closed-loop system in a standard MIMO feedback configuration [55], as illustrated in the block diagram in Fig. 3. We define the vector signals r, d_i, and d_o as exogenous; ξ_1, ξ_2, ξ_3, u, y, v as internal; and the system transfer functions, $\tilde{G}_P = (I_n - G_{T,P}G_{P,T})^{-1}(G_P + G_{T,P}G_T)$ and $\tilde{G}_T = (I_n - G_{P,T}G_{T,P})^{-1}(G_T + G_{P,T}G_P)$. Following the approach in [55], the internal transfer functions are obtained by

$$\begin{bmatrix}\xi_1 \\ \xi_2 \\ \xi_3\end{bmatrix} = \begin{bmatrix}I_{2n} & 0_{2n\times n} & F \\ -C & I_n & 0_{n\times 2n} \\ 0_{2n} & -G & I_{2n}\end{bmatrix}^{-1}\begin{bmatrix}r \\ d_i \\ d_o\end{bmatrix} \qquad (53)$$

where $G = [\tilde{G}_P;\ \tilde{G}_T]$, $C = [C_P W_P\ \ C_T]$, $F = [I_n\, 0_n;\ 0_n\, W_T]$. Twenty-five internal closed-loop transfer functions from $\hat{P}_g^{\text{ref}}$, r, d_i, $\tilde{q}_P$, and $\tilde{q}_T$ to e_P, e_T, P_g^{ref}, P_g, and F_T can be derived from (53). For conciseness, these functions are not explicitly presented. All transfer functions retain the characteristic matrix polynomial shown in (49). Moreover, they are well-defined and proper and have possible pole and zero cancellations inside the unit circle when satisfying the stability matrix conditions in (46) and (47). Consequently, Theorem 1 also ensures the internal stability of the closed-loop system based on these properties.

The robustness against output disturbances, which represents unmodeled effects and deviations from our identified

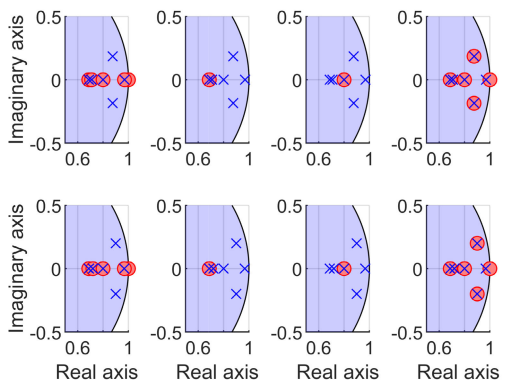

Fig. 4. Zero and pole mappings of the sensitivity function in our study case for the Central-WFC (upper subplots) and our proposed MCDC (down subplots). Slight dislocations are observed due to the delay in the MCDC formulation.

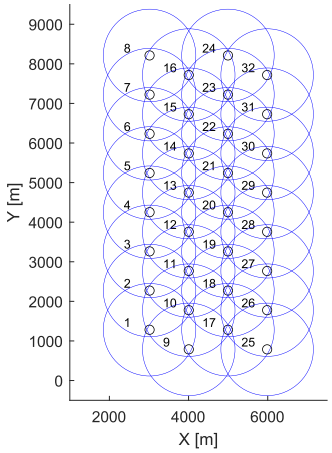

Fig. 5. Illustration of the communication range spanning $5(2)^{1/2}$ of the turbine diameter. In each blue circle, centered on the turbine location, communication is established with the enclosed turbines.

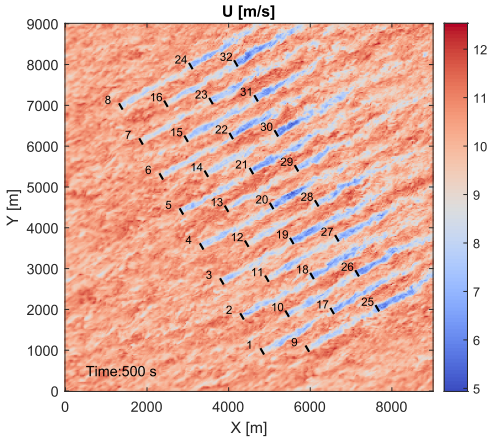

Fig. 6. Scenario 1—wind speed direction perpendicular to the TotalControl reference wind power plant [57].

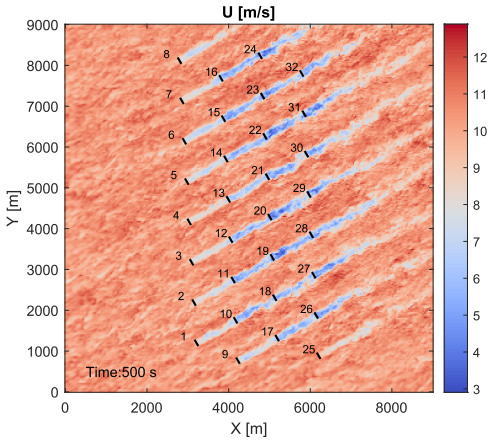

Fig. 7. Scenario 2—wind speed direction of 26.565° to the TotalControl reference wind power plant [57].

simplified WF model, is characterized by the output sensitivity transfer function from d_o to ξ_3, denoted as S and expressed as

$$S = (I_{2n} + GCF)^{-1} = \begin{bmatrix} I_n + \tilde{G}_P C_P W_P & \tilde{G}_P C_T W_T \\ \tilde{G}_T C_P W_P & I_n + G_T C_T W_T \end{bmatrix}^{-1}. \quad (54)$$

Norms are often employed for robustness analysis [55], but this approach can be computationally expensive and susceptible to numerical issues as our MIMO system scales with the number of turbines. As an alternative, we visually inspect the locations of the zeros and poles of the output sensitivity transfer function S. This process begins with the inverse operation utilizing block matrix inversion in (54). Then, the matrix polynomial equations are formulated from the numerator and the denominator of the derived four transfer functions as generalized eigenvalue problems [56] to find the zeros and poles, respectively. This approach is scalable for large numbers of turbines and higher-order system models.

In Fig. 4, we compare the zero and pole mappings of the four transfer functions derived from S using the MCDC formulation to those of the Central-WFC for our study case of 32 WTs. Considering the same control gains, we can see slight changes in the locations ofÂ the zeros and poles due to the different approaches. All poles are situated within the unit circle, characterizing stability, along with all zeros and possible cancellations. The greater the distance between the poles and zeros and the unit circle, the more robust the approach is. The poles of the MCDC shifted slightly to the right-hand side, indicating a minor reduction in robustness.

IV. Simulation Results

The proposed MCDC presented in Section III is evaluated in the high-fidelity large-eddy simulator SOWFA [58]. The WF layout is based on the TotalControl reference wind power plant [57] and the adopted set of neighbors $\mathcal{N}_i$ is set based on the communication range of each WT as depicted in Fig. 5. A low-wake interaction scenario (Scenario 1) and a medium-wake interaction scenario (Scenario 2) are considered, which differ in the prevailing wind direction, as illustrated in Figs. 6 and 7, respectively. The WF power reference is taken from a portion of the 40-min "RegD" test signal [59], normalized to have an amplitude of 32 MW with an additional persistent value of 112 MW. The simulations were set with a 10-Hz sampling rate, which was utilized in each WT power tracking controller, while a sampling rate of 2 Hz was implemented for the WF control. To reach an average consensus, we conservatively set the number of steps at $h = 400$, acknowledging that the WF control's sampling

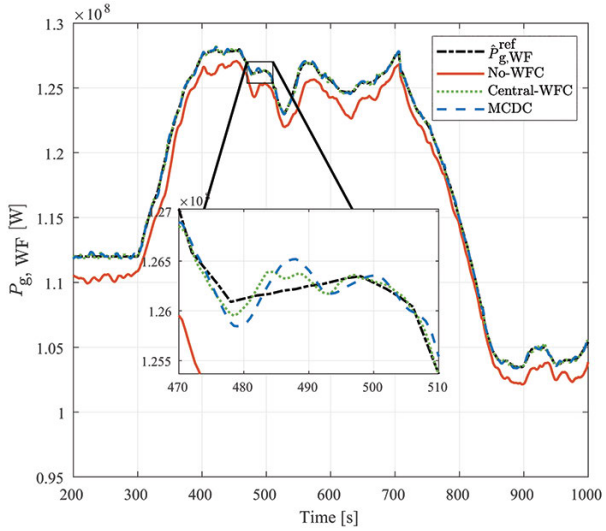

Fig. 8. WF active power generation in Scenario 1.

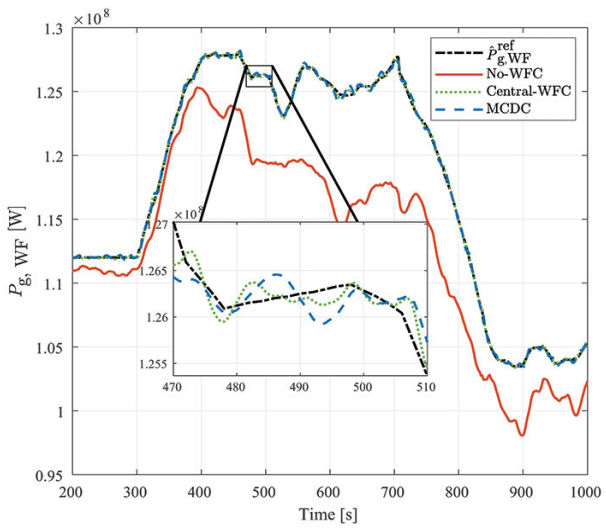

Fig. 9. WF active power generation in Scenario 2.

time does not necessitate the same level of swiftness as the WT control. This results in a communication rate of 800 Hz across the neighbor turbines, which is acceptable for typical low-range wireless communication devices.

The controller gains were selected as $K_P = (1/4)(1/n)$ and $K_T = 0.25$ based on insights from previous works [12], [16], and in accordance with theÂ stability conditions outlined in Theorem 1. The same values were applied in both the Central-WFC and the MCDC to assess the impacts of the introduced delays and the finite number of interactions to consensus from the MCDC approach.

We start by presenting the comparisons of the WF's active power generation, depicted in Fig. 8 for Scenario 1 and Fig. 9 for Scenario 2. The figures illustrate the power production of the WF over time which is regulated by a power demand from the operator. Both the central and the proposed distributed control approaches maintain the track of the WF power reference without an offset, in contrast to the observed offset in the absence of a WF controller (No-WFC). This offset results from the combination of power losses, where turbines generate less power than expected, caused by turbulence effects. Although compensation strategies in the open loop can help reduce this offset, turbine saturation further exacerbates this offset in Scenario 2, significantly impacting total power generation. A quantitative assessment of the WF's power tracking has been conducted and conveniently summarized in Table I. This evaluation is based on the root mean square error (RMSE) between the desired power reference and the actual power generation, as well as its peak error (PE). The key performance indicators are calculated from the 300-s mark onward. Despite the added delay from the average consensus computation, the MCDC showcases comparable performance when compared to the Central-WFC. Particularly, in Scenario 2, the MCDC achieves a 96.25% reduction in the RMSE of power compared with the No-WFC, which is comparable to the 97.65% reduction by the Central-WFC relative to the No-WFC.

Shifting our focus to the structural loads, the mean and standard deviation of the aerodynamic loads across the turbines are depicted in Fig. 10. A reduction in the standard deviation, illustrated by the shaded regions, is evident with the implementation of both the central and the proposed distributed control approaches. Again, it demonstrates equivalence between the approaches in balancing structural loads, in which the shaded region is reduced compared to the results from the No-WFC. The quantitative evaluation of the thrust balancers is additionally provided in Table I in terms of the mean and peak of the computed thrust force variance across the turbines. In Scenario 2, the MCDC achieves a 91.97% reduction in the mean of the thrust force variance, compared to the 92.29% reduction observed with the Central-WFC. Interestingly, in Scenario 1, with a reduction of 91.92% compared to 88.31% the MCDC overperforms the Central-WFC in the mean of the thrust force variance. This may seem counter-intuitive and it is ascribed to the inherent additional delay introduced by the MCDC, where we adopted the same gains in the controller from the Central-WFC. While the delay negatively impacts power compensation, it reflects positively on the thrust balancing, as the two loops exert opposing effects on each other. However, the control gains can be adjusted accordingly to balance these effects.

Our high-fidelity simulations examine the WF's ability to meet power demand using the proposed WF control strategy at an average wind speed of 10 ms^{-1} and a turbulence intensity of 5%–6% in the inflow. Nevertheless, it is important to acknowledge the limitations of our strategy in the following remark.

Remark 5: Rapid wind condition changes in real settings can affect the proposed design's performance, with consensus estimates diverging from current conditions. Reducing the WF sampling time can mitigate this, but it demands faster, yet feasible, communication. Low or no wind conditions can compromise WF power generation despite the controller's efforts. Managing volatility requires complementary strategies, such as energy storage and integrating wind with other energy sources.

TABLE I
PERFORMANCE OF WF CONTROLLERS

Scenario	Approach	RMSE of power [MW]	PE of power [MW]	Mean of thrust variance [GN^2]	Peak of thrust variance [GN^2]
1	No-WFC	1.2950	2.6982	2.3297	4.1050
	MCDC	0.1258	0.5536	0.1883	0.3881
	Central-WFC	0.1142	0.4612	0.2723	0.6272
2	No-WFC	6.0417	10.7650	8.0316	10.9100
	MCDC	0.2268	0.9006	0.6447	2.2425
	Central-WFC	0.1422	0.5021	0.6195	2.0546

*The cell colors range from light green for the lowest values to yellow for the highest values within each column.

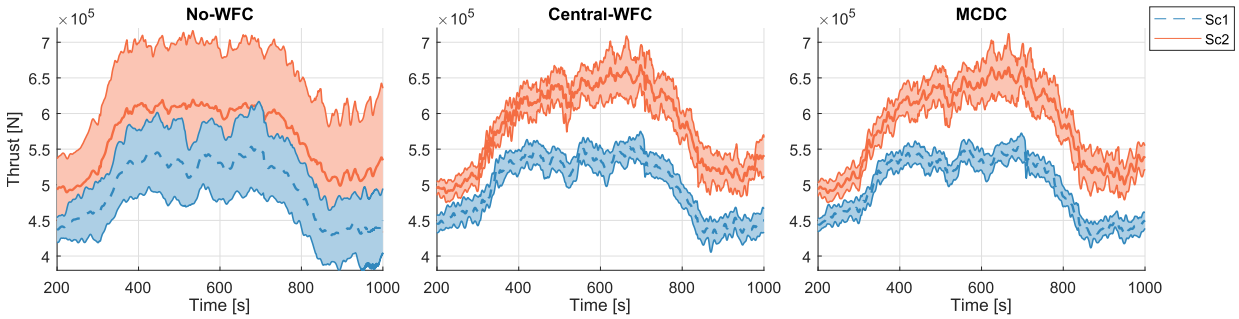

Fig. 10. Mean and standard deviation of thrust forces of all turbines in both Scenarios 1 and 2.

V. CONCLUSION

As wind parks transition toward large-scale systems, the prominent future trajectory for WF control is toward decentralization. However, this transformation introduces numerous challenges in effectively controlling the WTs cooperatively. This work presents the MCDC, a fully distributed control approach for power compensation, power distribution, and aerodynamic load balance. At a high rate, consensus is obtained for the variables of interest, and, at a low rate, the control takes place. This novel, practical approach integrates the WF objectives using well-established control methods, achieving effective results. The main advantages of the proposed MCDC framework include as follows.

1) MCDC does not rely on explicitly modeling WT interaction.
2) MCDC is both distributed and computationally tractable, facilitating straightforward implementation.
3) MCDC achieves performance comparable to the centralized controller.

Remarkably, the MCDC does not require a communication central point. This facilitates the implementation of WF control, which can be embedded locally in each WT. This paves the way for the production of WTs with WF control capabilities. Moreover, it requires only the current WT hardware and a short-distancing communication system, minimizing associated costs. While the MCDC relies on more frequent communication with neighboring WTs in comparison to the alternative approaches in the literature of distributed control, it is important to note that communication is limited to the neighboring WTs, and its performance matches the centralized controller.

As future venues of research, the proposed MCDC could be broadened to encompass additional applications in operation and management, such as distributing critical local structural information. Furthermore, the framework may prove advantageous for detecting cyber-attacks and corrupted signals within the communication channels. The high-rate layer utilized to reach consensus provides space to integrate detection algorithms, thus enhancing security and robustness against such malicious threats before actions are taken in the lower-rate layer. Additionally, extensions of this work include exploring strategies to accommodate link and node failures, as well as communication rate limitations. In these scenarios, consensus might not sufficiently converge within the sampling time of the WF control. The use of strategies that enhance convergence is of great value, such as robust network design and restarting mechanisms. Moreover, sufficient conditions for stability in the presence of extra delays are direct extensions of this work.

REFERENCES

[1] EirGrid. (2021). *Eirgrid Grid Code V. 10.0*. Accessed: Aug. 17, 2022. [Online]. Available: https://www.eirgridgroup.com/customer-and-industry/general-customer-information/grid-code-info

[2] ENTSO-E. (2019). *High Penetration of Power Electronic Interfaced Power Sources and the Potential Contribution of Grid Forming Converters*. Accessed: Apr. 18, 2023. [Online]. Available: https://www.entsoe.eu/publications/system-operations-reports/

[3] National Grid Electricity System Operator Limited. (2021). *The Grid Code*. Accessed: Apr. 18, 2023. [Online]. Available: https://www.nationalgrideso.com/industry-information/codes/grid-code-gc/grid-code-documents

[4] J. Aho, P. Fleming, and L. Y. Pao, "Active power control of wind turbines for ancillary services: A comparison of pitch and torque control methodologies," in *Proc. Amer. Control Conf. (ACC)*, Jul. 2016, pp. 1407–1412.

[5] K. Kim, H.-G. Kim, C.-J. Kim, I. Paek, C. L. Bottasso, and F. Campagnolo, "Design and validation of demanded power point tracking control algorithm of wind turbine," *Int. J. Precis. Eng. Manufacturing-Green Technol.*, vol. 5, no. 3, pp. 387–400, Jul. 2018.

[6] E. Ela et al., "Active power controls from wind power: Bridging the gaps," Nat. Renew. Energy Lab. (NREL), Tech. Rep., 2014.

[7] Y.-K. Wu, W.-H. Yang, Y.-L. Hu, and P. Q. Dzung, "Frequency regulation at a wind farm using time-varying inertia and droop controls," *IEEE Trans. Ind. Appl.*, vol. 55, no. 1, pp. 213–224, Jan. 2019.

[8] M. Tsili and S. Papathanassiou, "A review of grid code technical requirements for wind farms," *IET Renew. Power Gener.*, vol. 3, no. 3, pp. 308–332, Sep. 2009.
[9] F. Díaz-González, M. Hau, A. Sumper, and O. Gomis-Bellmunt, "Participation of wind power plants in system frequency control: Review of grid code requirements and control methods," *Renew. Sustain. Energy Rev.*, vol. 34, pp. 551–564, Jun. 2014.
[10] M. Vali, V. Petrović, G. Steinfeld, L. Y. Pao, and M. Kühn, "An active power control approach for wake-induced load alleviation in a fully developed wind farm boundary layer," *Wind Energy Sci.*, vol. 4, no. 1, pp. 139–161, Mar. 2019.
[11] J. G. Silva, B. Doekemeijer, R. Ferrari, and J.-W. van Wingerden, "Active power control of waked wind farms: Compensation of turbine saturation and thrust force balance," in *Proc. Eur. Control Conf. (ECC)*, Jun. 2021, pp. 1223–1228.
[12] J. Gonzalez Silva, R. Ferrari, and J.-W. Van Wingerden, "Wind farm control for wake-loss compensation, thrust balancing and load-limiting of turbines," *Renew. Energy*, vol. 203, pp. 421–433, Feb. 2023.
[13] T. Knudsen, T. Bak, and M. Svenstrup, "Survey of wind farm control—Power and fatigue optimization," *Wind Energy*, vol. 18, no. 8, pp. 1333–1351, 2015.
[14] S. Siniscalchi-Minna, F. D. Bianchi, C. Ocampo-Martinez, J. L. Domínguez-García, and B. De Schutter, "A non-centralized predictive control strategy for wind farm active power control: A wake-based partitioning approach," *Renew. Energy*, vol. 150, pp. 656–669, May 2020.
[15] D. Wald, J. King, C. J. Bay, R. Chintala, and K. Johnson, "Integration of distributed controllers: Power reference tracking through charging station and building coordination," *Appl. Energy*, vol. 314, May 2022, Art. no. 118753.
[16] J.-W. van Wingerden, L. Pao, J. Aho, and P. Fleming, "Active power control of waked wind farms," *IFAC-PapersOnLine*, vol. 50, no. 1, pp. 4484–4491, 2017.
[17] J. Aho et al., "A tutorial of wind turbine control for supporting grid frequency through active power control," in *Proc. Amer. Control Conf. (ACC)*, Jun. 2012, pp. 3120–3131.
[18] J. Annoni, P. M. O. Gebraad, A. K. Scholbrock, P. A. Fleming, and J. V. Wingerden, "Analysis of axial-induction-based wind plant control using an engineering and a high-order wind plant model," *Wind Energy*, vol. 19, no. 6, pp. 1135–1150, Jun. 2016.
[19] D. van der Hoek, S. Kanev, J. Allin, D. Bieniek, and N. Mittelmeier, "Effects of axial induction control on wind farm energy production—A field test," *Renew. Energy*, vol. 140, pp. 994–1003, Sep. 2019.
[20] P. Fleming et al., "Continued results from a field campaign of wake steering applied at a commercial wind farm – part 2," *Wind Energy Sci.*, vol. 5, no. 3, pp. 945–958, Jul. 2020.
[21] S. Tamaro and C. L. Bottasso, "A new wind farm active power control strategy to boost tracking margins in high-demand scenarios," in *Proc. Amer. Control Conf. (ACC)*, May 2023, pp. 192–197.
[22] A. Croce, S. Cacciola, and F. Isella, "Combining wake redirection and derating strategies in a load-constrained wind farm power maximization," *Wind Energy Sci.*, vol. 9, no. 5, pp. 1211–1227, May 2024.
[23] J. W. van Wingerden et al., "Expert elicitation on wind farm control," *J. Phys., Conf. Ser.*, vol. 1618, no. 2, Sep. 2020, Art. no. 022025.
[24] S. Boersma, B. M. Doekemeijer, S. Siniscalchi-Minna, and J. W. van Wingerden, "A constrained wind farm controller providing secondary frequency regulation: An LES study," *Renew. Energy*, vol. 134, pp. 639–652, Apr. 2019.
[25] P. Fleming, J. Aho, P. Gebraad, L. Pao, and Y. Zhang, "Computational fluid dynamics simulation study of active power control in wind plants," in *Proc. Amer. Control Conf. (ACC)*, Jul. 2016, pp. 1413–1420.
[26] F. Fele, J. M. Maestre, and E. F. Camacho, "Coalitional control: Cooperative game theory and control," *IEEE Control Syst. Mag.*, vol. 37, no. 1, pp. 53–69, Feb. 2017.
[27] V. N. Coelho, M. W. Cohen, I. M. Coelho, N. Liu, and F. G. Guimarães, "Multi-agent systems applied for energy systems integration: State-of-the-art applications and trends in microgrids," *Appl. Energy*, vol. 187, pp. 820–832, Feb. 2017.
[28] M. J. Ghadi, A. Rajabi, S. Ghavidel, A. Azizivahed, L. Li, and J. Zhang, "From active distribution systems to decentralized microgrids: A review on regulations and planning approaches based on operational factors," *Appl. Energy*, vol. 253, Nov. 2019, Art. no. 113543.
[29] H. Liang, B. J. Choi, W. Zhuang, and X. Shen, "Stability enhancement of decentralized inverter control through wireless communications in microgrids," *IEEE Trans. Smart Grid*, vol. 4, no. 1, pp. 321–331, Mar. 2013.
[30] F. Dörfler, J. W. Simpson-Porco, and F. Bullo, "Breaking the hierarchy: Distributed control and economic optimality in microgrids," *IEEE Trans. Control Netw. Syst.*, vol. 3, no. 3, pp. 241–253, Sep. 2016.
[31] C. J. Bay, R. Chintala, V. Chinde, and J. King, "Distributed model predictive control for coordinated, grid-interactive buildings," *Appl. Energy*, vol. 312, Apr. 2022, Art. no. 118612.
[32] F. Dörfler, M. R. Jovanović, M. Chertkov, and F. Bullo, "Sparsity-promoting optimal wide-area control of power networks," *IEEE Trans. Power Syst.*, vol. 29, no. 5, pp. 2281–2291, Sep. 2014.
[33] Y. E. Hawas and H. S. Mahmassani, "Comparative analysis of robustness of centralized and distributed network route control systems in incident situations," *Transp. Res. Record, J. Transp. Res. Board*, vol. 1537, no. 1, pp. 83–90, Jan. 1996.
[34] T. Keijzer and R. M. G. Ferrari, "Threshold design for fault detection with first order sliding mode observers," *Automatica*, vol. 146, Dec. 2022, Art. no. 110600.
[35] J. R. Marden, S. D. Ruben, and L. Y. Pao, "A model-free approach to wind farm control using game theoretic methods," *IEEE Trans. Control Syst. Technol.*, vol. 21, no. 4, pp. 1207–1214, Jul. 2013.
[36] P. M. O. Gebraad and J. W. van Wingerden, "Maximum power-point tracking control for wind farms," *Wind Energy*, vol. 18, no. 3, pp. 429–447, Mar. 2015.
[37] J. Park and K. H. Law, "A data-driven, cooperative wind farm control to maximize the total power production," *Appl. Energy*, vol. 165, pp. 151–165, Mar. 2016.
[38] Z. Dong, Z. Li, Z. Liang, Y. Xu, and Z. Ding, "Distributed neural network enhanced power generation strategy of large-scale wind power plant for power expansion," *Appl. Energy*, vol. 303, Dec. 2021, Art. no. 117622.
[39] J. Annoni et al., "A framework for autonomous wind farms: Wind direction consensus," *Wind Energy Sci. Discuss.*, vol. 2018, pp. 1–17, Oct. 2018.
[40] F. Bernardoni, U. Ciri, M. A. Rotea, and S. Leonardi, "Identification of wind turbine clusters for effective real time yaw control optimization," *J. Renew. Sustain. Energy*, vol. 13, no. 4, Jul. 2021, Art. no. 043301.
[41] H. M. Al-Rahmani and G. F. Franklin, "Multirate control: A new approach," *Automatica*, vol. 28, no. 1, pp. 35–44, Jan. 1992.
[42] M. Tomizuka, "Multi-rate control for motion control applications," in *Proc. 8th IEEE Int. Workshop Adv. Motion Control (AMC)*, Nov. 2004, pp. 21–29.
[43] R. Olfati-Saber, J. A. Fax, and R. M. Murray, "Consensus and cooperation in networked multi-agent systems," *Proc. IEEE*, vol. 95, no. 1, pp. 215–233, Jan. 2007.
[44] A. Jadbabaie, J. Lin, and A. S. Morse, "Coordination of groups of mobile autonomous agents using nearest neighbor rules," *IEEE Trans. Autom. Control*, vol. 48, no. 6, pp. 988–1001, Jun. 2003.
[45] V. Spudić, C. Conte, M. Baotić, and M. Morari, "Cooperative distributed model predictive control for wind farms," *Optim. Control Appl. Methods*, vol. 36, no. 3, pp. 333–352, May 2015.
[46] P. Daoutidis, M. Soroush, and C. Kravaris, "Feedforward/feedback control of multivariable nonlinear processes," *AIChE J.*, vol. 36, no. 10, pp. 1471–1484, Oct. 1990.
[47] J. Alvarez-Ramirez, A. Morales, and I. Cervantes, "Robust proportional-integral control," *Ind. Eng. Chem. Res.*, vol. 37, no. 12, pp. 4740–4747, 1998.
[48] Z. P. Jiang and I. Marcels, "Robust nonlinear integral control," *IEEE Trans. Autom. Control*, vol. 46, no. 8, pp. 1336–1342, Aug. 2001.
[49] J. G. Silva, B. M. Doekemeijer, R. Ferrari, and J.-W.-V. Wingerden, "Active power control of wind farms: An instantaneous approach on waked conditions," *J. Phys., Conf. Ser.*, vol. 2265, no. 2, May 2022, Art. no. 022056.
[50] W. Ren, H. Chao, W. Bourgeous, N. Sorensen, and Y. Chen, "Experimental validation of consensus algorithms for multivehicle cooperative control," *IEEE Trans. Control Syst. Technol.*, vol. 16, no. 4, pp. 745–752, Jul. 2008.
[51] L. Xiao and S. Boyd, "Fast linear iterations for distributed averaging," *Syst. Control Lett.*, vol. 53, no. 1, pp. 65–78, Sep. 2004.
[52] E. Jury, *Theory and Applications of the Z-Transform Method*. New York, NY, USA, 1964.
[53] E. I. Jury, "A simplified stability criterion for linear discrete systems," *Proc. IRE*, vol. 50, no. 6, pp. 1493–1500, Jun. 1962.
[54] M. Andreasson, D. V. Dimarogonas, H. Sandberg, and K. H. Johansson, "Distributed control of networked dynamical systems: Static feedback, integral action and consensus," *IEEE Trans. Autom. Control*, vol. 59, no. 7, pp. 1750–1764, Jul. 2014.
[55] J. Doyle, B. Francis, and A. Tannenbaum, *Feedback Control Theory*. New York, NY, USA: Macmillan, 1992.
[56] C. B. Moler and G. W. Stewart, "An algorithm for generalized matrix eigenvalue problems," *SIAM J. Numer. Anal.*, vol. 10, no. 2, pp. 241–256, Apr. 1973.
[57] S. Andersen et al. (2018). *Reference Wind Power Plant*. Accessed: Aug. 17, 2022. [Online]. Available: https://orbit.dtu.dk/en/publications/reference-wind-power-plant-d103
[58] (2020). *SOWFA Data-Driven Control(TU Delft)*. Accessed: Aug. 17, 2022. [Online]. Available: https://github.com/TUDelft-DataDrivenControl/SOWFA
[59] C. Pilong, *PJM Manual 12: Balancing Operations*, 30th ed., Audubon, PA, USA: PJM, 2013.